[9]K. S. Krane, C. E. Olsen, J. R. Sites, and W. A. Steyert, Phys. Rev. Letters 26, 1579 (1971).
[10]P. Limon, L. Pondrum, S. Olsen, P. Kloeppel, R. Handler, and S. C. Wright, Phys. Rev. 169, 1026 (1968).
[11]E. H. Thorndike, Phys. Rev. 138, 586 (1965).
[12]E. J. Gucker, Ph.D. thesis, University of Rochester, 1970 (unpublished).
[13]A. E. Woodruff, Ann. Phys. (N.Y.) 7, 65 (1959).

PHYSICAL REVIEW D VOLUME 4, NUMBER 9 1 NOVEMBER 1971

Charge-Exchange Production Mechanism for $K^*(890)$†

G. C. Fox
Lauritsen Laboratory of Physics, California Institute of Technology, Pasadena, California 91109

and

R. Engelmann, B. Musgrave, F. Schweingruber, and H. Yuta
Argonne National Laboratory, Argonne, Illinois 60439

and

B. Forman, N. Gelfand, and H. Schulz
Enrico Fermi Institute, University of Chicago, Chicago, Illinois 60637
(Received 13 May 1971)

We present new results on $K^-p \to K^-\pi^+ n$ at 5.5 GeV/c. We fit all the available $d\sigma/dt$ and decay density-matrix elements for the $K^{\pm}N \to K^{*0}N$ charge-exchange reactions. The difference between the K^+ and K^- reactions is explained successfully in terms of interference between a ρ Regge pole and strong absorptive corrections to the π Regge pole. This difference is related by vector dominance (VDM) to the π^+ and π^- photoproduction cross sections and polarized-photon asymmetry data. The VDM predictions are only qualitatively successful.

I. INTRODUCTION

Previous studies of the charge-exchange reactions[1,2]

$$K^-p \to \bar{K}^{*0}(890)n\,, \tag{1}$$

$$K^+n \to K^{*0}(890)p \tag{2}$$

have indicated that one-pion exchange (OPE) represents a significant component of the production mechanism. A reasonable description of the data at a given energy is provided by the absorptive OPE model.[3] Another approach suggested by Schlein uses the OPE model with corrections for off-mass-shell effects given by Dürr-Pilkuhn form factors.[4] Although the data at each energy for (1) have generally been sparse, there is good agreement between the density matrices for the $\bar{K}^*(890)$; the differential cross section for $|t|<0.5$ (GeV/c)^2 is consistent with the form $d\sigma/dt = Ae^{Bt}$, where $B \sim 5$ (GeV/c)$^{-2}$.[5] The data for reaction (2) are restricted to a few energies, but it seems clear that its cross section is larger than that of (1) at the same momentum and also that the differential cross section is *more* peripheral than is observed for (1). In this paper, we discuss an explicit model for K^* production. We show that the difference in the slope of $d\sigma/dt$ for the K^- and K^+ reactions is obtained naturally in an absorption model using Reggeized π and ρ exchange.

II. EXPERIMENTAL RESULTS

First, to illustrate the salient feature of (1), we refer to new results[6] at 5.5 GeV/c obtained from measurement of about 40 000 two-prong events in the ANL 30-in. bubble chamber. Track measurement and ionization determinations were done using POLLY[7] with subsequent automatic hypothesis assignments in the kinematical fitting program. A detailed analysis of these measurements will appear later, but we stress here that particular attention was directed at the problem of contamination of

$$K^-p \to K^-\pi^+n \tag{3}$$

by misidentification of the processes

$$K^-p \to \pi^+\pi^-(\Lambda^0/\Sigma^0)\,, \tag{4}$$

which we estimate is less than 7% of the total se-

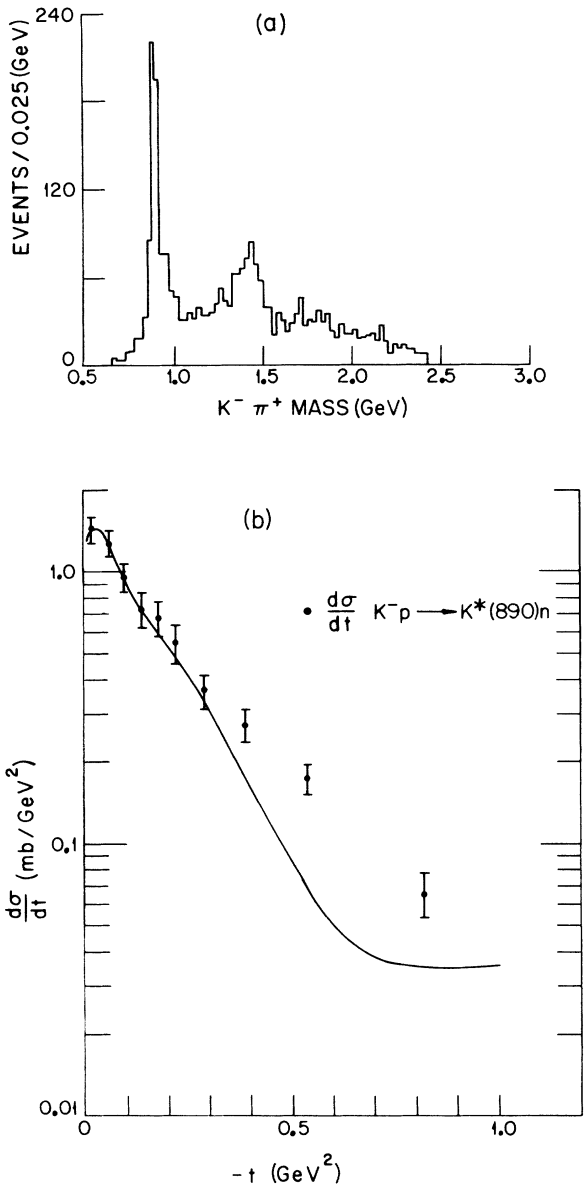

FIG. 1. (a) The $K^-\pi^+$ mass distribution, (b) $d\sigma/dt$ for $\bar{K}^*(890)$ production for the reaction $K^-p \to K^-\pi^+ n$ at 5.5 GeV/c. The curve was obtained from the absorption-model fit described in the text.

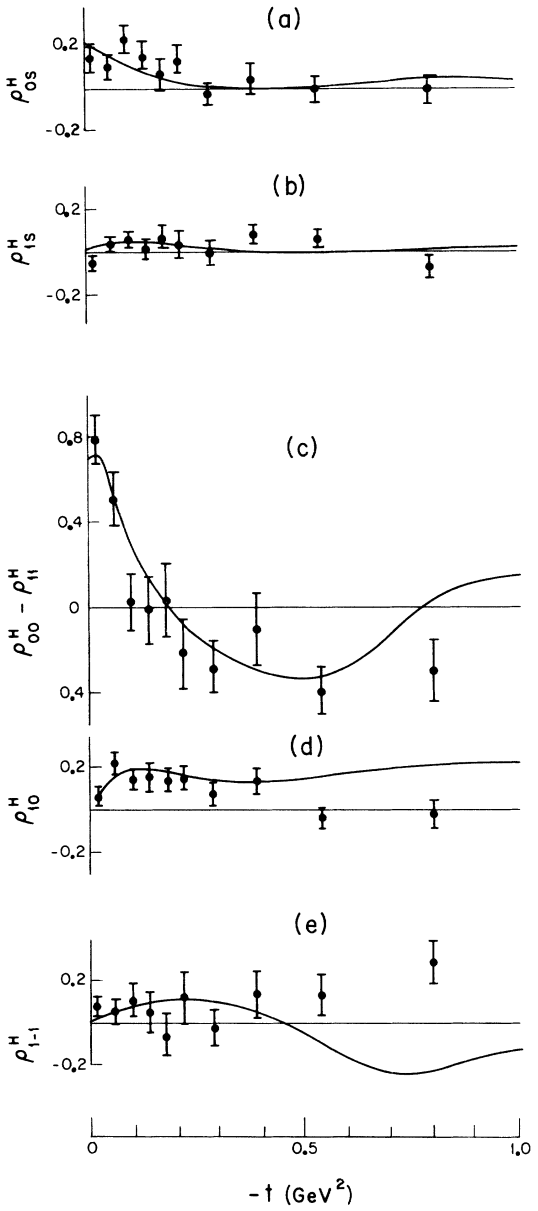

FIG. 2. (a)-(e) Density-matrix elements for $\bar{K}^{*0}$ in the helicity frame for $K^-p \to \bar{K}^*(890)n$ at 5.5 GeV/c. The curves were obtained from the absorption-model fit described in the text.

lected events for reaction (3) and is only 2% in the $\bar{K}^*(890)$ region.[8]

The cross section for reaction (3) is measured to be 832 ± 41 μb.[3] The detailed features are presented in Fig. 1. The mass distribution in Fig. 1(a) shows, as at other energies, prominent peaks corresponding to the strong production of $\bar{K}^{*0}(890)$ and $\bar{K}^{*0}(1420)$ resonances.

Turning to the production and decay characteristics of $\bar{K}^{*0}(890)$, we show the differential cross section in Fig. 1(b). The $\bar{K}^{*0}$ cross section,[9] corrected for unseen decays, is 380 ± 48 μb. The slight reduction in the differential cross section at small momentum transfer is removed when the distribution in $t' = t - t_{\min}$ (not shown) is considered. For $|t| < 0.5$ (GeV/c)^2, the slope of the differential cross section is 4.75 ± 0.50 (GeV/c)$^{-2}$. The pronounced forward-backward asymmetry observed in the polar decay angular distribution of the $\bar{K}^{*0}(890)$ indicates that both S- and P-wave com-

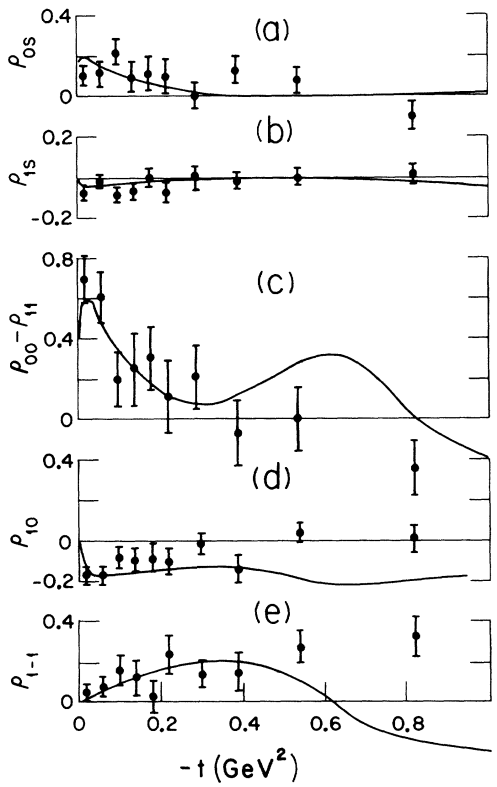

FIG. 3. (a)-(e) Density-matrix elements for $\bar{K}^{*0}$ in the Gottfried-Jackson frame for $K^-p \to \bar{K}^*(890)n$ at 5.5 GeV/c. The curves show the result of the absorption-model fit described in the text.

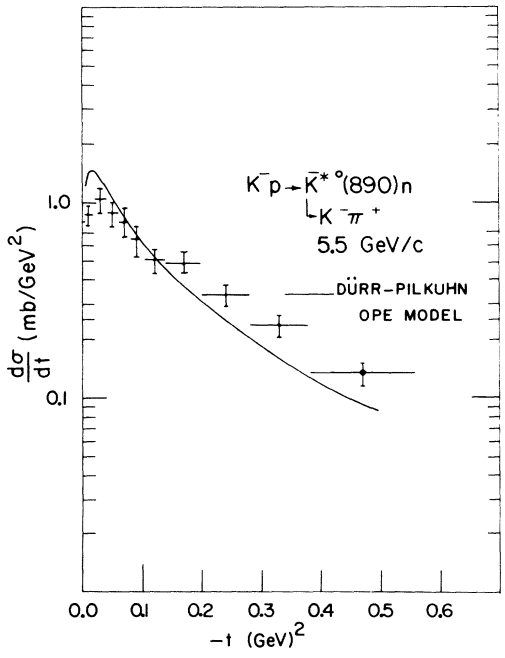

FIG. 4. The $d\sigma/dt$ for $K^-p \to \bar{K}^{*0}(890)n$ at 5.5 GeV/c compared to the Dürr-Pilkuhn-model prediction as given in Ref. 4.

ponents of the $K\pi$ system are important, and we have used this parametrization of the density matrix. The s-channel (helicity frame) density-matrix elements are shown in Figs. 2(a)–2(e) while the corresponding t-channel (Gottfried-Jackson) quantities are presented in Figs. 3(a)–3(e). The density-matrix elements and $d\sigma/dt$ values are given in Tables I–III. We note here that the Dürr-Pilkuhn OPE model would predict that $\rho_{00}=1$ and that the differential cross section for both the K^-p and the K^+n reactions would be identical, contrary to observation. In Fig. 4 we compare the $d\sigma/dt$ predicted by this model with the present data at 5.5 GeV/c. The parameters were taken from Ref. 4. With increasing t, the data fall off less quickly than the model would indicate.

In either frame, the large values of $|\mathrm{Re}\rho_{10}|$ and ρ_{11} near the forward direction indicate that strong absorption is needed to describe the data. Further, we note that the t dependence (dips, breaks, etc.) of s- and t-channel amplitudes is reflected in the density-matrix elements evaluated in, respectively, the s- and t-channel frames. Whereas in the strong-cut Reggeized absorption model[10] (SCRAM) the s-channel amplitudes have a distinctive structure, exchange (Regge-pole) effects are naturally associated with t-channel amplitudes. In both frames we note that $\rho_{00}-\rho_{11}$ decreases rapidly in value away from the forward direction (pion pole), indicating that non-pion-exchange processes are important. It is most accurate to study the product of the density-matrix elements with $d\sigma/dt$, and

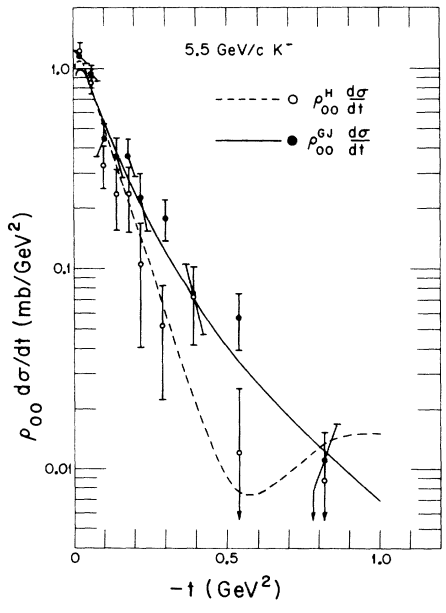

FIG. 5. $\rho_{00}^H\ d\sigma/dt$ and $\rho_{00}^{GJ}\ d\sigma/dt$ for the $\bar{K}^{*0}$ in $K^-p \to \bar{K}^*(890)n$ at 5.5 GeV/c with curves from the absorption-model fit.

TABLE I. Differential cross sections.[a]

t range (GeV^2)	Number of events	$d\sigma/dt$ (mb/GeV^2)
0.0–0.02	40	1.297 ±0.137
0.02–0.04	48	1.557 ±0.150
0.04–0.06	41	1.330 ±0.138
0.06–0.08	37	1.200 ±0.131
0.08–0.10	30	0.973 ±0.118
0.10–0.14	47	0.762 ±0.074
0.14–0.20	69	0.746 ±0.060
0.20–0.28	63	0.509 ±0.043
0.28–0.38	54	0.350 ±0.032
0.38–0.56	55	0.198 ±0.018
0.56–1.0	52	0.0769 ±0.007

[a] The mass range $0.84 \leq M(K^-\pi^+) \leq 0.94$ GeV/c^2 is used to define the $K^*(890)$ and to obtain the numbers in the table. The differential cross section is normalized to the cross section for $K^-p \to \bar{K}^{*0}(890)n$ corrected for unseen decay modes.

in Fig. 5 we compare $\rho_{00}^{GJ}d\sigma/dt$ and $\rho_{00}^{H}d\sigma/dt$.[11] There is a striking difference in the slopes of these t distributions: As we already mentioned, the slope parameter for $d\sigma/dt$ is 4.75 ± 0.5 (GeV/c)$^{-2}$, to be contrasted with those for $\rho_{00}^{GJ}d\sigma/dt$ and $\rho_{00}^{H}d\sigma/dt$ of 7.4 ± 0.8 and 12.1 ± 1.3 (GeV/c)$^{-2}$, respectively. Whereas $d\sigma/dt$ is much flatter than that for the typical OPE process $\pi N \to \rho N$, the t dependence of $\rho_{00}d\sigma/dt$ is similar for K^* and ρ production. For instance, in $\pi^-p \to \rho^0 n$ at 8 GeV/c, $d\sigma/dt$, $\rho_{00}^{GJ}d\sigma/dt$, and $\rho_{00}^{H}d\sigma/dt$ have slopes 10.9 ± 0.5, 10.9 ± 0.6, and 13.6 ± 1.0 (GeV/c)$^{-2}$, respectively.[12] The SCRAM model of Ross *et al.* predicts a dip in $\rho_{00}^{H}d\sigma/dt$ at $|t| \sim 0.5$ (GeV/c)^2 in all such vector-meson production experiments. This is an unambiguous prediction for any amount of π, B, and natural parity (ρ, A_2) exchange. One need only make the presumably safe assumption that A_1 exchange is negligible. The present data do not show conclusive evidence for this zero, although it is encouraging for the SCRAM model that $\rho_{00}^{H}d\sigma/dt$ is sharper than $\rho_{00}^{GJ}d\sigma/dt$. A comprehensive survey of the dip structure in $\rho_{00}^{H}d\sigma/dt$ at $t \approx -0.6$ (GeV/c)^2 in $\bar{K}N \to \bar{K}^*N$, $\pi N \to \rho N$, and $\pi N \to \omega N$ is contained in Ref. 13.

III. VECTOR DOMINANCE FOR $\rho_{11}d\sigma/dt$

In the above we have demonstrated empirically that the anomalously small slope for $\bar{K}^{*0}$ production is associated with the dominance of $2\rho_{11}^{H}d\sigma/dt$ at large $-t$. Let us now show that this is expected from a combination of SU_3 and the vector-dominance model (VDM).[14] Explicitly we have the relation

$$2\rho_{11}^{H}\frac{d\sigma}{dt}(K^-p \to \bar{K}^{*0}n) - 2\rho_{11}^{H}\frac{d\sigma}{dt}(K^+n \to K^{*0}p) = \chi\left(\frac{d\sigma}{dt}(\gamma p \to \pi^+ n) - \frac{d\sigma}{dt}(\gamma n \to p\pi^-)\right), \tag{5}$$

where $\chi = 3\gamma_\rho^2/\alpha\pi$, $\alpha = 1/137$, and γ_ρ is the universal ρ-meson coupling constant. Figs. 6(a), 6(b), and 6(c) plot R_γ for the reasonable value $\gamma_\rho^2/4\pi = 0.45$.[15]

$$R_\gamma = e^{-4t}(\tfrac{1}{5}E_{\text{lab}})^2\chi\left(\frac{d\sigma}{dt}(\gamma p \to n\pi^+) - \frac{d\sigma}{dt}(\gamma n \to p\pi^-)\right) \tag{6}$$

at $E_{\text{lab}} = 5$, 8, and 16 GeV. The figures indicate that (6) is essentially independent of energy. The e^{-4t} factor is inserted to remove the t dependence of the $\bar{K}^{*0}$ data and Figs. 7(a) and 7(b) show R_K for comparison.

$$R_K = e^{-4t}(\tfrac{1}{5}P_{\text{lab}})^2 2\rho_{11}^{H}\frac{d\sigma}{dt} \tag{7}$$

for K^{*0} and $\bar{K}^{*0}$ production at 3 and 5.5 GeV/c, re-

TABLE II. Helicity-frame density-matrix elements.[a]

t range (GeV^2)	Number of events	$\rho_{00}^{H} - \rho_{11}^{H}$	Re ρ_{10}^{H}	Re $\rho_{1,-1}^{H}$	ρ_{0S}^{H}	ρ_{1S}^{H}
0.0–0.02	40	1.00 ±0.18	0.01 ±0.06	0.13 ±0.06	0.30 ±0.10	−0.06 ±0.04
0.02–0.04	48	0.62 ±0.17	0.13 ±0.07	0.04 ±0.08	0.03 ±0.09	−0.03 ±0.04
0.04–0.06	41	0.44 ±0.20	0.16 ±0.07	0.09 ±0.10	0.12 ±0.09	0.03 ±0.05
0.06–0.08	37	0.58 ±0.17	0.29 ±0.07	0.00 ±0.09	0.10 ±0.10	0.06 ±0.05
0.08–0.10	30	0.09 ±0.18	0.09 ±0.08	0.11 ±0.12	0.22 ±0.09	0.10 ±0.06
0.10–0.14	47	−0.03 ±0.16	0.17 ±0.06	0.08 ±0.09	0.28 ±0.06	0.07 ±0.05
0.14–0.20	69	0.00 ±0.14	0.16 ±0.05	−0.02 ±0.08	0.06 ±0.06	0.02 ±0.04
0.20–0.28	63	−0.33 ±0.12	0.13 ±0.05	0.01 ±0.09	0.07 ±0.05	0.05 ±0.05
0.28–0.38	54	−0.12 ±0.15	0.10 ±0.06	0.11 ±0.10	0.04 ±0.07	0.07 ±0.05
0.38–0.56	55	−0.24 ±0.13	0.00 ±0.05	0.15 ±0.09	−0.05 ±0.06	0.04 ±0.05
0.56–1.00	52	−0.39 ±0.12	−0.01 ±0.06	0.24 ±0.09	0.03 ±0.06	−0.04 ±0.05

[a] The helicity (s-channel) frame is defined in the $K^*(890)$ rest system with the z axis opposite to the direction of the recoil neutron and with the $\hat{y}$ axis along the direction $\hat{y} = \hat{K}_{\text{in}}^- \times \hat{K}_{\text{out}}^* / |\hat{K}_{\text{in}}^- \times \hat{K}_{\text{out}}^*|$.

TABLE III. Jackson-frame density-matrix elements.[a]

t range (GeV^2)	Number of events	$\rho_{00}^{GJ}-\rho_{11}^{GJ}$	Re ρ_{10}^{GJ}	Re $\rho_{1,-1}^{GJ}$	ρ_{0S}^{GJ}	Re ρ_{1S}^{GJ}
0.0–0.02	40	0.819 ± 0.187	−0.209 ± 0.061	0.069 ± 0.064	0.256 ± 0.094	−0.118 ± 0.039
0.02–0.04	48	0.611 ± 0.169	−0.138 ± 0.067	0.037 ± 0.080	−0.002 ± 0.089	−0.044 ± 0.043
0.04–0.06	41	0.483 ± 0.179	−0.146 ± 0.079	0.106 ± 0.089	0.116 ± 0.091	−0.029 ± 0.046
0.06–0.08	37	0.744 ± 0.200	−0.199 ± 0.069	0.060 ± 0.067	0.124 ± 0.103	−0.012 ± 0.046
0.08–0.10	30	0.099 ± 0.211	−0.079 ± 0.076	0.112 ± 0.102	0.254 ± 0.084	−0.053 ± 0.059
0.10–0.14	47	0.275 ± 0.169	−0.079 ± 0.059	0.179 ± 0.088	0.244 ± 0.073	−0.120 ± 0.039
0.14–0.20	69	0.289 ± 0.133	−0.090 ± 0.058	0.076 ± 0.090	0.052 ± 0.067	−0.032 ± 0.038
0.20–0.28	63	0.269 ± 0.152	−0.038 ± 0.048	0.209 ± 0.072	0.084 ± 0.069	−0.029 ± 0.036
0.28–0.38	54	−0.030 ± 0.160	−0.094 ± 0.056	0.135 ± 0.088	0.096 ± 0.066	−0.023 ± 0.045
0.38–0.56	55	−0.060 ± 0.156	0.006 ± 0.054	0.211 ± 0.076	0.058 ± 0.066	0.032 ± 0.042
0.56–1.0	52	−0.144 ± 0.136	−0.006 ± 0.058	0.326 ± 0.083	−0.063 ± 0.065	−0.006 ± 0.040

[a]The Jackson (t-channel) frame is defined in the $K^*(890)$ rest system with the z axis along the incident K^- direction and with the y axis along the direction $\hat{y}=\hat{K}_{in}^{-}\times\hat{K}_{out}^{*}/|\hat{K}_{in}^{-}\times\hat{K}_{out}^{*}|$.

spectively.[16] Correspondingly, Eq. (5) predicts that the difference between the $\bar{K}^{*0}$ and K^{*0} curves is equal to the photoproduction quantity (6).

The small value of R_γ near the forward direction predicts the equality of R_K for K^{*0} and $\bar{K}^{*0}$ near $t=0$. This does not seem to be indicated by the data of Figs. 7(a) and 7(b), and although it is probably a real physical effect, we ignore such questions of normalization here. Instead we plot in Fig. 7(c) the difference $R(\bar{K}^{*0})-R(K^{*0})$ with the K^{*0} data renormalized to equal the $\bar{K}^{*0}$ data at $t=0$. This is to be compared with R_γ, represented by the dashed line in Fig. 7(c). There is a qualitative agreement with VDM although the quantitative comparison is wrong by, say, a factor of 2 (photoproduction is too big). It would be good to confirm this, at higher energies, with K^{*0} and $\bar{K}^{*0}$ data at the same energy and with well-determined relative normalization. In particular we remark that the energy independence of (6) suggests that there should be a large difference between the K^{*0} and $\bar{K}^{*0}$ production cross sections and a flat slope of $\bar{K}^{*0}d\sigma/dt$ up to at least 16 GeV/c. This is a sensitive test of VDM and it is important to check it in hadronic experiments.

IV. VECTOR DOMINANCE FOR $\rho_{1,-1}\,d\sigma/dt$

There is a well-known[14] VDM relation for polarized photons. Letting $\Sigma^{\pm}$ be the usual polarized-photon asymmetries in $\pi^{\pm}$ photoproductions, it reads

$$2\rho_{1,-1}^{H}\frac{d\sigma}{dt}(\pi^-p\to\rho^0n)+\tfrac{2}{9}\rho_{1,-1}^{H}\frac{d\sigma}{dt}(\pi^+n\to\omega^0p)=\frac{1}{3}\left(\Sigma^{+}\frac{d\sigma}{dt}(\gamma p\to n\pi^+)+\Sigma^{-}\frac{d\sigma}{dt}(\gamma n\to p\pi^-)\right)\chi\,.$$

One can easily derive an SU_3 analog of this corresponding to Eq. (5). Let

$$\bar{R}_\gamma=e^{-4t}(\tfrac{1}{5}E_{lab})^2\chi\left(\Sigma^{+}\frac{d\sigma}{dt}(\gamma p\to n\pi^+)-\Sigma^{-}\frac{d\sigma}{dt}(\gamma n\to p\pi^-)\right), \tag{8}$$

and for the hadronic data

$$\bar{R}_K=e^{-4t}(\tfrac{1}{5}P_{lab})^2 2\rho_{1,-1}^{H}\frac{d\sigma}{dt}\,. \tag{9}$$

Then vector dominance predicts

$$\bar{R}(\bar{K}^{*0})-\bar{R}(K^{*0})=\bar{R}_\gamma\,. \tag{10}$$

Figure 8 shows $\bar{R}_\gamma$; Fig. 9(a), $\bar{R}(K^{*0})$; Fig. 9(b), $\bar{R}(\bar{K}^{*0})$; and Fig. 9(c), the difference $\bar{R}(\bar{K}^{*0})-\bar{R}(K^{*0})$. Here the open circles in 9(c) represent $\bar{R}_\gamma$ and this figure again indicates a substantial quantitative violation of vector dominance. As before, the hadronic data are too small – the discrepancy (say a factor of 4) being rather larger than in the $2\rho_{11}^{H}d\sigma/dt$ comparison of Fig. 7(c).

Similar disagreement with VDM has been found in a recent $\pi^-p\to\rho^0n$ experiment at 15 GeV/c.[17] Again the hadronic cross sections were lower than the VDM prediction away from $t=0$, while the ratio $\rho_{1,-1}/\rho_{11}$ was also smaller than predicted.

In spite of the quantitative disagreement with VDM, Figs. 7(c) and 9(c) confirm the qualitative interpretation of the $\bar{K}^{*0}$, K^{*0} cross-section difference and smaller $\bar{K}^{*0}$ slope with the same mechanism that causes the difference between π^+ and π^- photoproduction. We now turn to a consideration of this within an explicit model.

V. ABSORPTION MODEL

We have previously proposed an absorption model[18] involving other Regge-pole exchanges besides the π, which not only explains the K^* data but also

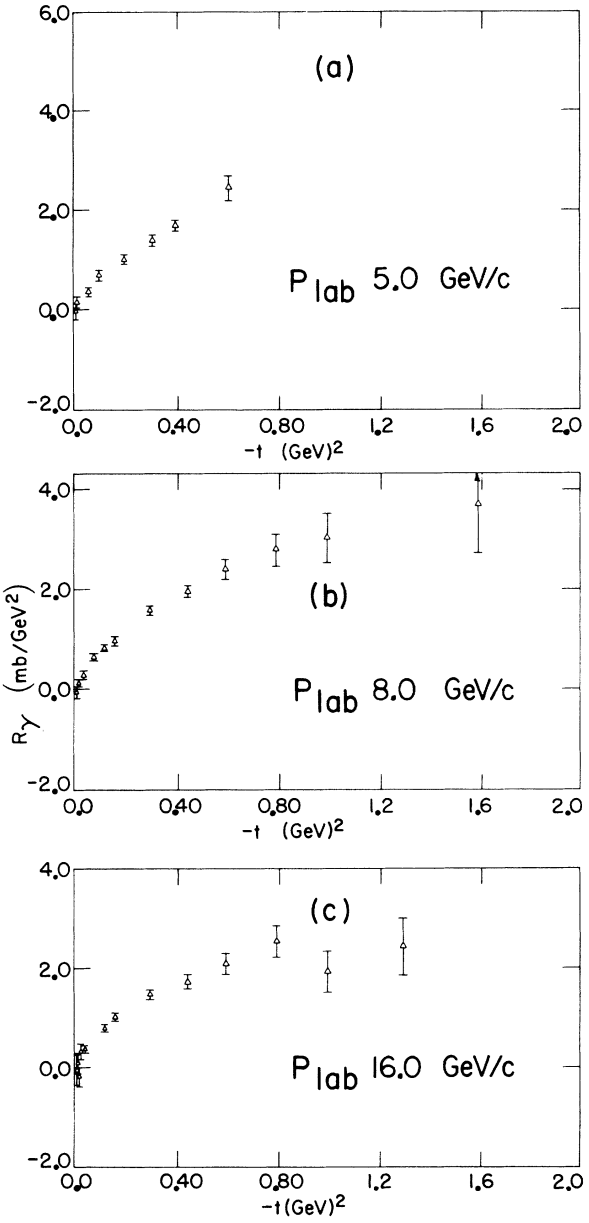

FIG. 6. $R_\gamma = e^{-4t}(\frac{1}{5}E_{lab})^2 \chi[d\sigma/dt(\gamma p \to \pi^+ n) - d\sigma/dt(\gamma n \to \pi^- p)]$ with $\chi = 3\gamma_\rho^2/\alpha\pi$ for (a) $E_{lab} = 5$, (b) 8, and (c) 16 GeV.

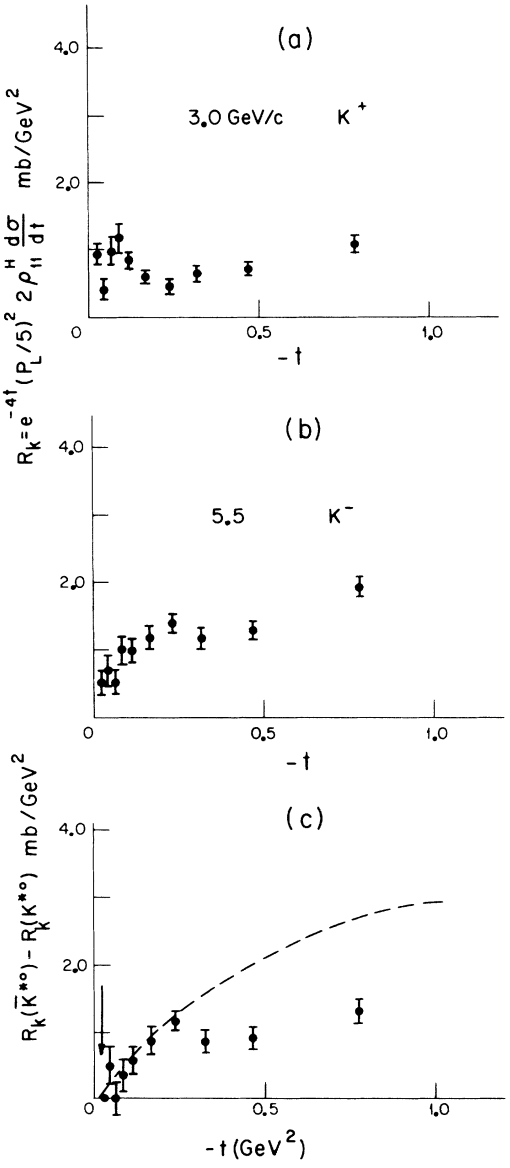

FIG. 7. (a), (b) R_K for K^{*0} and $\bar{K}^{*0}$ at 3 and 5.5 GeV/c, respectively, (c) the difference between the $\bar{K}^{*0}$ and K^{*0} data in (a) and (b), where $R_K = e^{-4t}(\frac{1}{5}P_{lab})^2 2\rho_{11}^H \, d\sigma/dt$. The first data point for the K^{*0} is normalized to the $\bar{K}^{*0}$ data at the point indicated by the arrow.

relates it to other line-reversed reactions.[19] In view of the possible existence of systematic errors in the different experiments, we will not discuss here the tricky question of difference in size between the $\bar{K}^{*0}$ and K^{*0} data[20] but rather consider the difference in slope. In accordance with the VDM considered above, we obtain this from the interference of the ρ Regge pole with the strong (SCRAM) cut correction to π exchange.

The formalism and qualitative features of the SCRAM model have been well described in Ref. 10. In the Appendix, we detail our realization of this model for K^* production and also define the independent parameters. We employed π, ρ, and A_2 exchange[21] and determined these parameters by fitting all available $\bar{K}^{*0}$ and K^{*0} data.[22] The fitted values of the parameters are recorded in Table IV. Both the S- and P-wave components of the $K\pi$ sys-

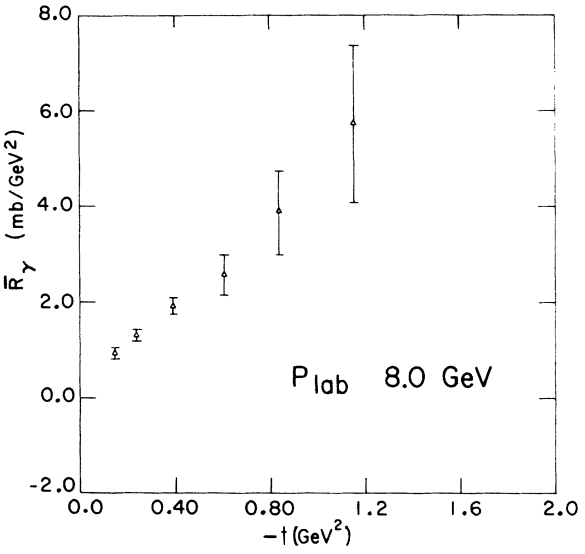

FIG. 8. $\bar{R}_\gamma = e^{-4t}(\frac{1}{5}E_{1ab})^2\chi[\Sigma^+ d\sigma/dt(\gamma p \to n\pi^+) - \Sigma^- d\sigma/dt(\gamma n \to p\pi^-)]$, with $\chi = 3\gamma_\rho{}^2/\alpha\pi$ at $E_{1ab} = 8$ GeV.

tem were included in the fit. Assuming resonant P-wave and $K\pi$ scattering ($\delta_P = 90°$), the fit determines the on-shell S-wave $K\pi$ phase shift $\delta_S = 64° \pm 10°$ at the K^* mass. The fit is compared with $d\sigma/dt$ for $K^-p \to \bar{K}^{*0}n$ in Fig. 10(a) and $K^+n \to K^{*0}p$ in Fig. 10(b). (To be exact, we plot $e^{-4t}(\frac{1}{5}P_{lab})^2 d\sigma/dt$.[23]) The fit is quite satisfactory considering the relatively small number of parameters. The good fit to the t-channel density-matrix elements is shown in Figs. 3(a)–3(e) for $K^-p \to \bar{K}^{*0}n$ at 5.5 GeV/c and in Figs. 11(a)–11(e) for $K^+n \to K^{*0}p$ at 3 GeV/c. The comparison with the s-channel density-matrix elements in Figs. 2(a)–2(e) shows the characteristic

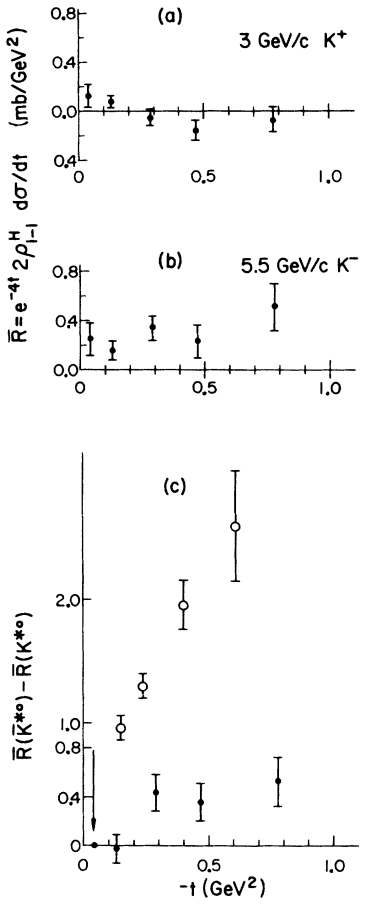

FIG. 9. (a) $\bar{R}(K^{*0})$ for $K^+n \to K^*(890)p$ at 3 GeV/c, (b) $\bar{R}(\bar{K}^{*0})$ for $K^-p \to \bar{K}^*(890)n$ at 5.5 GeV/c, (c) $\bar{R}(\bar{K}^{*0}) - \bar{R}(K^{*0})$, where $\bar{R}_K = e^{-4t}(\frac{1}{5}P_{1ab})^2 2\rho^H_{1,-1}\, d\sigma/dt$.

TABLE IV. Parameters of fit. S-wave absorption constant $C = 1.354$. Pole parameters.

Vertex	Coupling	Value of γ	Fixed parameters
	(1) π Regge pole: $\alpha = -0.0196 + t$		
$\bar{N}N$	γ_{++}	-33.67	-33.67 [a]
$K\bar{K}^*$ (P-wave)	γ_{00}	$(2.17 - 27.46t)e^{-0.258t}$	-27.46 [b]
	γ_{01}	$(29.17 - 8.12t)e^{-0.258t}$	-8.12 [b]
$K\bar{K}^*$ (S-wave)	γ_{00}	1.11	
	(2) ρ Regge pole: $\alpha = 0.5 + 0.9t$		
$\bar{N}N$	γ_{++}	-80	
	γ_{+-}	-320	-320 [c]
$K\bar{K}^*$ (P-wave)	γ_{01}	$1e^{1.0t}$	1 [a]
	(3) A_2 Regge pole: $\alpha = 0.5 + 0.9t$		
$\bar{N}N$	γ_{++}	-60	
	γ_{+-}	-240	-240 [c]
$K\bar{K}^*$ (P-wave)	γ_{01}	$1e^{2.5t}$	1 [a]

[a] Parameter fixed arbitrarily as only product $\gamma_{\bar{N}N}\gamma_{K\bar{K}^*}$ determined by fit.
[b] Parameter fixed by threshold constant (Ref. 28).
[c] Parameter fixed from known flip/nonflip ratio from $\pi^-p \to \pi^0 n$, etc. analysis.

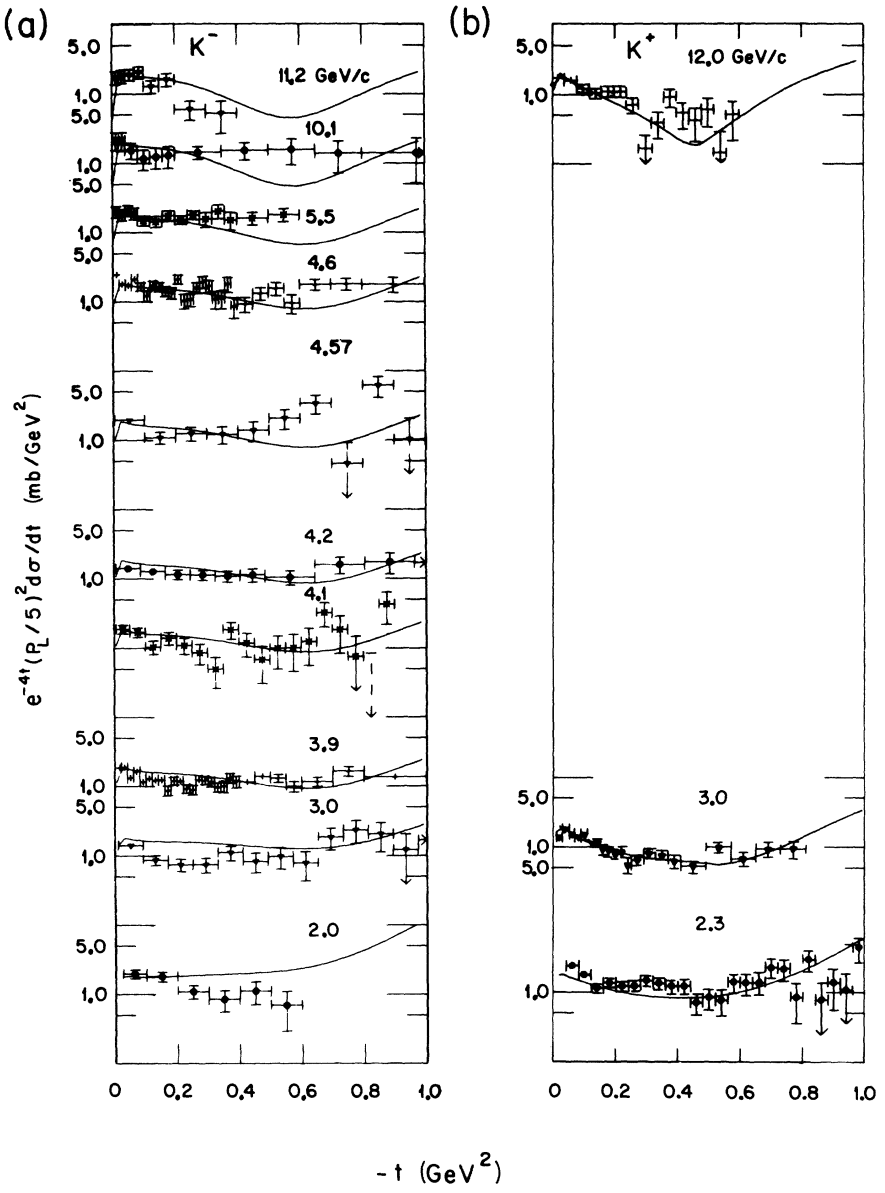

FIG. 10. (a) $e^{-4t}(\frac{1}{5}P_{1ab})^2 d\sigma/dt$ for $K^-p \to \bar{K}^*(890)n$, (b) $e^{-4t}(\frac{1}{5}P_{1ab})^2 d\sigma/dt$ for $K^+n \to K^*(890)p$. The curves show the result of the absorption-model fit described in the text.

SCRAM structure in $\rho_{00} - \rho_{11}$ discussed in the first part of the paper. This is further illustrated in Figs. 5 and 12, which show $\rho^H_{00} d\sigma/dt$ and $\rho^{GJ}_{00} d\sigma/dt$ for $\bar{K}^{*0}$ and K^{*0} at 5.5 and 3 GeV/c, respectively.[24] These show the dip at $t \approx -0.5$ (GeV/c)^2 expected in any s-channel single-flip cross section (as in the π-exchange contribution $\rho^H_{00} d\sigma/dt$ to $KN \to K^*N$ or $\pi N \to \rho N$) from the SCRAM model.[10] One would also naively expect a zero in $\mathrm{Re}\rho^H_{10}$ near this t value [≈ -0.5 (GeV/c)^2], but the model calculations for $\bar{K}^{*0}$ [Fig. 2(d)] and K^{*0} (not shown) show a featureless $\mathrm{Re}\rho^H_{10}$ in this region. This is due to the "SCRAM zero" being in different positions, namely $t = -0.4$ and -0.8 (GeV/c)^2, for the real and imaginary parts of the π-exchange amplitude. This prediction should perhaps not be taken too seriously as it is sensitive to many omissions,[25] e.g., B exchange, in the model at large $-t$ values. Nevertheless, it is comforting that the natural prediction of a dip in $\rho^H_{00} d\sigma/dt$ is *not* affected by these technical points. Finally, the projected cross sections $d\sigma/dt$ and $\rho^H_{00} d\sigma/dt$ at 12, 17, and 40 GeV/c are shown in Fig. 13.

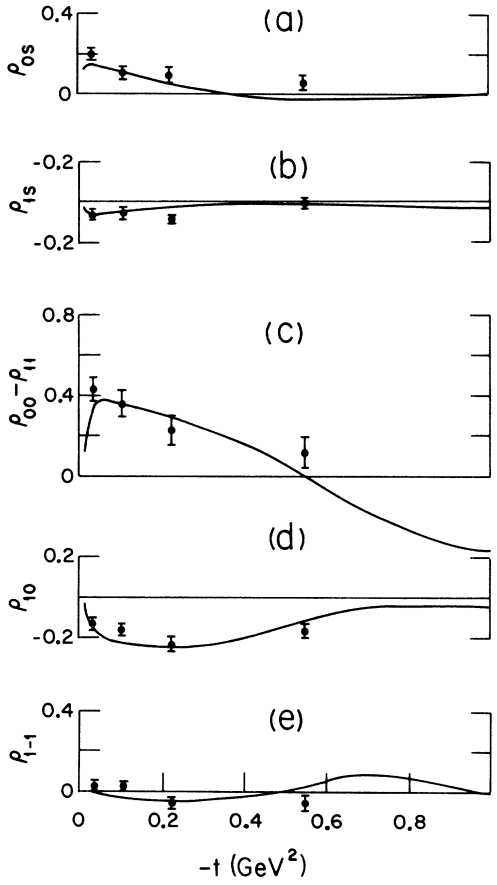

FIG. 11. (a)-(e) Density-matrix elements in the Gottfried-Jackson frame for $K^+n \to K^*(890)p$ at 3 GeV/c. The curves were obtained from the absorption-model fit described in the text.

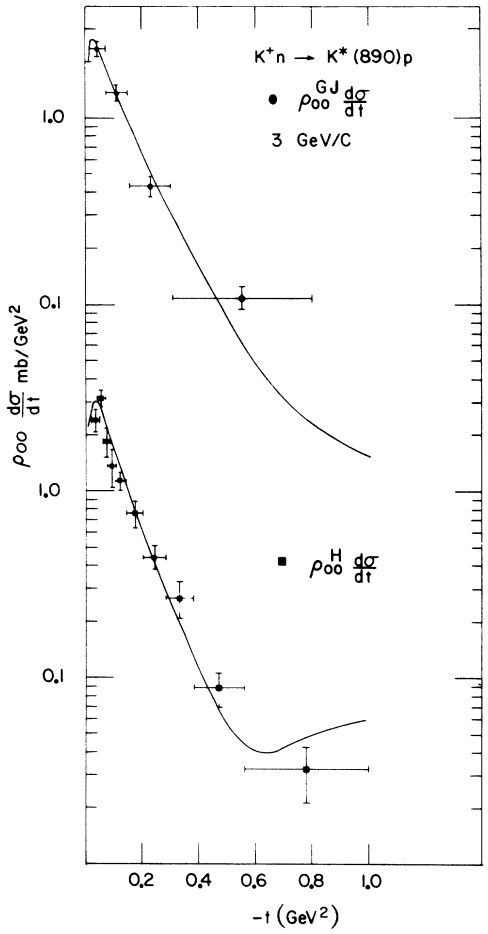

FIG. 12. $\rho_{00}^{H}\, d\sigma/dt$ and $\rho_{00}^{GJ}\, d\sigma/dt$ for $K^+n \to K^*(890)p$ at 3 GeV/c with curves showing the result of the absorption-model fit described in the text.

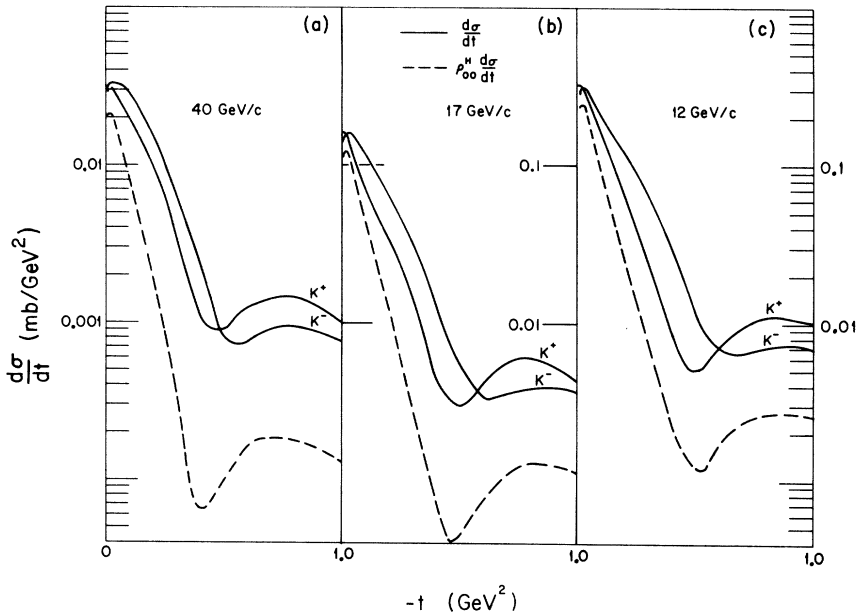

FIG. 13. Predictions of the model for $d\sigma/dt$, K^{*0}, $\bar{K}^{*0}$, and $\rho_{00}^{H}\, d\sigma/dt$ (same for K^{*0} and $\bar{K}^{*0}$ in our model) at (a) 40 GeV/c, (b) 17 GeV/c, and (c) 12 GeV/c. The 40-GeV/c prediction should be related to the left-hand scale.

VI. CONCLUSION

In conclusion, we have shown that the qualitative features of K^* production are in agreement with simple theoretical ideas. Decisive tests of the explicit model and the vector-dominance predictions await data of higher statistics at preferably higher energies and with a detailed treatment of the relative normalization of $\bar{K}^{*0}$ and K^{*0} data. Independently of any model, a systematic experimental study of the t dependence of $\rho d\sigma/dt$ for the various vector-meson production reactions ($\pi N \to \rho N$, $KN \to K^*N$, $\pi N \to \omega N$, $\pi N \to \rho\Delta$, $KN \to K^*\Delta$, $\pi N \to \omega\Delta$) will be very fruitful.

ACKNOWLEDGMENTS

We acknowledge helpful discussions on the SCRAM model with G. Kane. We also acknowledge the help and interest of M. Derrick and E. Berger. Finally, we are grateful to A. Angelopoulos, R. L. Eisner, A. Firestone, and W. Wittek for the generous provision of unpublished data.

APPENDIX: THEORETICAL FORMALISM

Let $H^s_{\mu_1\mu_2\to\mu_3\mu_4}(s,t)$ be the usual[26] s-channel helicity amplitudes for the process $1+2\to 3+4$ with respective helicities μ_i. In our case $1=K$, $\bar{K}$; $2=n$, p; $3=K^*$, $\bar{K}^*$ (S and P waves); $4=p,n$. We now define the Fourier-Bessel partial-wave amplitudes $h_{\mu_1\mu_2\to\mu_3\mu_4}(s,b)$, in terms of which we can define the absorption model as[10,12,27]

$$h_{\text{final}}(s,b)=h_{\text{Regge pole}}(s,b)[1-C\exp(-b^2/2a)]. \tag{A1}$$

a, the slope of elastic scattering, was fixed at 8 $(\text{GeV}/c)^{-2}$ in the fit presented here. C, the S-wave absorption constant, is a free parameter. We now must specify the unabsorbed Regge-pole amplitude $h_{\text{Regge pole}}(s,b)$. This is done in terms of t-channel amplitudes $H^t_{\lambda_1\lambda_3\to\lambda_2\lambda_4}(s,t)$, which are related to the s-channel amplitudes by[26]

$$H^s_{\mu_1\mu_2\to\mu_3\mu_4}(s,t)=\sum_{\lambda_1\lambda_2\lambda_3\lambda_4} H^t_{\lambda_1\lambda_3\to\lambda_2\lambda_4}(s,t)\exp[i\pi(s_3-s_2+\mu_1+\mu_2+\mu_3+\mu_4)]d^{s_1}_{\lambda_1\mu_1}(\chi_1)d^{s_2}_{\lambda_2\mu_2}(\chi_2)d^{s_3}_{\lambda_3\mu_3}(\chi_3)d^{s_4}_{\lambda_4\mu_4}(\chi_4), \tag{A2}$$

where the crossing angles χ_1 through χ_4 are chosen to lie between 0 and π and are defined by

$$\cos\chi_1=\frac{(s+m_1^2-m_2^2)(t+m_1^2-m_3^2)+2m_1^2\Delta}{S_{12}T_{13}},$$

$$\cos\chi_2=\frac{-(s+m_2^2-m_1^2)(t+m_2^2-m_4^2)+2m_2^2\Delta}{S_{12}T_{24}},$$

$$\cos\chi_3=\frac{-(s+m_3^2-m_4^2)(t+m_3^2-m_1^2)+2m_3^2\Delta}{S_{34}T_{13}}, \tag{A3}$$

$$\cos\chi_4=\frac{(s+m_4^2-m_3^2)(t+m_4^2-m_2^2)+2m_4^2\Delta}{S_{34}T_{24}},$$

with

$$\Delta=m_3^2+m_2^2-m_1^2-m_4^2,$$

$$S_{12}^2=[s-(m_1-m_2)^2][s-(m_1+m_2)^2],$$

$$T_{13}^2=[t-(m_1-m_3)^2][t-(m_1+m_3)^2], \text{ etc.}$$

To specify our sign and normalization conventions we note that for meson-baryon scattering

$$d\sigma/dt=\frac{0.3893}{(64\pi m_N P_{\text{lab}}^2)}\sum|H|^2, \tag{A4}$$

where the sum runs over the 6 (2) independent amplitudes for P- (S-) wave $KN\to K^*N$ or $\bar{K}N\to\bar{K}^*N$ scattering. The density-matrix elements for the K^* ($\bar{K}^*$) are given as

$$\rho_{\lambda_3\lambda_3'}\propto\sum_{\lambda_1\lambda_2\lambda_4}\epsilon_{\lambda_3\lambda_3'}H_{\lambda_1\lambda_2\lambda_3\lambda_4}(s,t)\times H^*_{\lambda_1\lambda_2\lambda_3\lambda_4}(s,t), \quad [\text{Tr}(\rho)=1], \tag{A5}$$

where for helicity-frame density-matrix elements we use $\epsilon=1$ and $H=H^s$ and for Jackson-frame density-matrix elements, $H=H^t$ and $\epsilon=(-1)^{\lambda_3-\lambda_3'}$.

We now must complete our painful definitions by specifying the parametrization of the t-channel amplitudes. With $\lambda_i=\lambda_1-\lambda_3$, $\lambda_f=\lambda_2-\lambda_4$ we write for each Regge pole

$$H^t_{\lambda_1\lambda_3\to\lambda_2\lambda_4}=F_{\text{CG}}\otimes F_{\text{PRB}}(s,t,\lambda_i,\lambda_f)\otimes F_{\text{SIG}}(t,\alpha)\otimes\exp[i\pi(\lambda_2+\lambda_3)]\otimes Y_{\lambda_1\lambda_3}(t)\otimes Y_{\lambda_2\lambda_4}(t)\otimes\nu^\alpha, \qquad \nu=\tfrac{1}{2}(s-u) \tag{A6}$$

where the Clebsch-Gordan factor

$$F_{\text{CG}}=+1 \quad \text{all poles: } K^-p\to\bar{K}^{*0}n \quad \text{and } \rho\text{: } K^+n\to K^{*0}p; \tag{A7}$$

$$F_{\text{CG}}=-1 \quad \pi, A_2\text{: } K^+n\to K^{*0}p.$$

The physical-region boundary factor

$$F_{\text{PRB}}(s,t,\lambda_i,\lambda_f)=[(1+Z)/Z_a]^{|\lambda_i+\lambda_f|/2}\otimes[(Z-1)/Z_a]^{|\lambda_i-\lambda_f|/2} \tag{A8a}$$

is asymptotically unity but ensures the correct behavior at the physical-region boundary at finite energies. Here

$$Z=[2\nu t+(m_1^2-m_3^2)(m_2^2-m_4^2)]/(T_{13}T_{24}) \quad \text{(A8b)}$$

is the t-channel scattering cosine and

$$Z_a=2\nu t/(T_{13}T_{24}) \quad \text{(A8c)}$$

its asymptotic form.

The signature factor $F_{\mathrm{SIG}}(\tau,\alpha)$ (τ = signature, α = trajectory) in the reported fit took the form[27]:

$$F_{\mathrm{SIG}}(+,\alpha)=-(e^{-i\pi\alpha}+1)/[2\sin\pi\alpha\,\Gamma(\tfrac{1}{2}(\alpha+2))]\,,$$
$$F_{\mathrm{SIG}}(-,\alpha)=-(e^{-i\pi\alpha}-1)/[2\sin\pi\alpha\,\Gamma(\tfrac{1}{2}(\alpha+1))]\,. \quad \text{(A9)}$$

Finally, the residues Y are related to the parametrized kinematic singularity-free residues γ by

$$Y_{\lambda_k\lambda_l}=K_{\lambda_k\lambda_l}\gamma_{\lambda_k\lambda_l}\,, \quad \text{(A10)}$$

and K takes the following form.

(1) *$\bar{N}N$ vertex.*

$$\rho,\ A_2\colon\ K_{++}=N\,,\ K_{+-}=\sqrt{-t}N\,;$$
$$\pi\colon\qquad K_{++}=-\sqrt{-t}\,,\ K_{+-}=0\,. \quad \text{(A11)}$$

(2) *$K\bar{K}^*$ vertex (P wave).*

$$\rho,\ A_2\colon\ K_{00}=0\,,\ K_{01}=-\sqrt{-t}N\,;$$
$$\pi\colon\qquad K_{00}=1/T_{13}\,,\ K_{01}=\alpha\sqrt{-t}/T_{13}\,. \quad \text{(A12)}$$

(3) *$K\bar{K}^*$ vertex (S wave).*

$$\rho,\ A_2\colon\ K_{00}=0\,;$$
$$\pi\colon\qquad K_{00}=1 \quad \text{(A13)}$$

with the nonsense factor $N=\sqrt{\alpha}$ for A_2 and $N=1$ for ρ.

We parametrize the $\gamma_{\lambda_k\lambda_l}$ subject to the two threshold constraints for the $\pi\to K\bar{K}^*$ (P-wave) vertex.[28] The fitted values of C and the independent γ's are recorded in Table IV.

---

†Work supported by the U.S. Atomic Energy Commission and by the National Science Foundation.

[1]For further references to reaction (1) see Y. W. Kang, Phys. Rev. 176, 1587 (1968).

[2]I. Butterworth *et al.*, Phys. Rev. Letters 15, 737 (1965); CERN-Brussels-Munich collaboration, Nucl. Phys. B16, 125 (1970).

[3]F. S. Schweingruber *et al.*, Phys. Rev. 166, 1317 (1968).

[4]P. Schlein, *Meson Spectroscopy*, edited by C. Baltay and A. H. Rosenfeld (Benjamin, New York, 1968), p.161.

[5]Compilation of data by G. C. Fox:

$K^+n\to K^{*0}p$. 2.3 GeV/c: S. Goldhaber *et al.*, Phys. Rev. Letters 15, 737 (1965). 3 GeV/c: G. Bassompierre *et al.*, Nucl. Phys. B16, 125 (1970); W. Wittek, private communication to G. C. Fox. 12 GeV/c: A. Firestone, private communication to B. Musgrave.

$K^-p\to K^{*0}n$. 2 GeV/c: M. Dickerson *et al.*, Phys. Letters 23, 505 (1966). 3 GeV/c: J. Goldberg *et al.*, Phys. Letters 30B, 434 (1969); J. Badier *et al.*, Saclay Report No. CEA-R 3037, 1966 (unpublished); A. Verglas *et al.*, Nuovo Cimento 41, 629 (1966); A. Rouge, thesis, Ecole Polytechnique, 1968 (unpublished). 3.5 GeV/c: BGLRO collaboration, Rutherford Laboratory Report No. RPP/H/29 (unpublished). 3.9 and 4.6 GeV/c: M. Aguilar-Benitez *et al.*, Phys. Rev. Letters 24, 466 (1971); M. Aguilar-Benitez and R. L. Eisner, private communication to G. C. Fox. 4.1 GeV/c: F. L. Schweingruber *et al.*, Phys. Rev. 166, 1317 (1968). 4.2 GeV/c: Nijmegen-Amsterdam Collaboration, paper contributed to the Fifteenth International Conference on High Energy Physics, Kiev, U.S.S.R., 1970 (unpublished). 4.57 GeV/c: Y. W. Kang, Phys. Rev. 176, 1587 (1968). 5.5 GeV/c: This paper. 10.1 GeV/c: M. Aderholz *et al.*, Nucl. Phys. B5, 567 (1968); B7, 111 (1968); and A. Angelopoulos, private communication to B. Musgrave.

[6]These results represent the completion of the analysis referred to in Ref. 3. The detailed account of the experimental analysis of the complete sample is being prepared for publication.

[7]W. W. M. Allison *et al.*, Nucl. Instr. Methods 84, 129 (1970).

[8]Consideration of this problem is also contained in Ref. 3. Contamination from channels other than $K^-p\to\pi^+\pi^-\Lambda$ is estimated to be less than 7%.

[9]Resonance cross sections were estimated by fitting the complete channel $K^-\pi^+n$ using a maximum-likelihood method.

[10]M. Ross *et al.*, Nucl. Phys. B23, 269 (1970).

[11]We calculated ρ_{00} from $\rho_{00}-\rho_{11}$ using the trace condition $\rho_{00}-2\rho_{11}=1$. We ignore the S-wave background for not only is it a small effect, but also the models predict a similar t-dependence for $\rho_{00}d\sigma/dt$ and the S-wave.

[12]We thank W. Selove for permission to use the 8-GeV/c π^-p data.

[13]G. C. Fox, in *Phenomenology in Particle Physics 1971*, edited by C. B. Chiu, G. C. Fox, and A. J. G. Hey (California Institute of Technology, Pasadena, Calif., 1971).

[14]A. Bialas and K. Zalewski, Nucl. Phys. B6, 483 (1968); A. Bialas, A. Gula, B. Muryn, and K. Zalewski, Phys. Letters 26B, 513 (1968); M. Krammer and D. Schildknecht, Nucl. Phys. B7, 583 (1968).

[15]I. Derado *et al.*, Phys. Rev. Letters 21, 1556 (1968).

[16]For clarity we show the $\bar{K}^{*0}$ data at only one energy. Similar results are obtained from the other experiments listed in Ref. 5.

[17]F. Bulos *et al.*, SLAC Report No. SLAC-PUB-885, 1971 (unpublished).

[18]R. Engelmann *et al.*, paper contributed to the Fifteenth International Conference on High Energy Physics, Kiev, U.S.S.R., 1970 (unpublished).

[19]K.-W. Lai and J. Louie, Nucl. Phys. B19, 205 (1970). A recent review of the systematics of line-reversed processes is given by C. B. Chiu, in Proceedings of the Workshop on Particle Physics at Intermediate Energies,

Lawrence Radiation Laboratory report, 1971 (unpublished).

[20]A preliminary discussion of the size of K^{*0} and $\bar{K}^{*0}$ data can be found in Ref. 18.

[21]We have considered various models involving B exchange, conspiring trajectories, and/or various amounts of absorption in the K^+ and K^- channels. The fit presented here uses equal absorption in the K^+ and K^- channels. Putting in the expected differences in the absorption for the K^+ reactions gives a poorer fit. Thus the absorption sharpens the t distribution of the K^-p reaction to cancel the π-ρ interference effect. A detailed study of this and other models will be presented elsewhere.

[22]We varied a total of nine parameters, namely, the absorption constant and a total of eight coupling constants. The model was fitted to the $\bar{K}^{*0}$ data above 3.6 GeV/c and the K^{*0} data above 2.5 GeV/c.

[23]We took some account of the normalization differences between the various experiments by allowing in $d\sigma/dt$ an over-all t-independent renormalization to be determined by the fit. We used 0.71 for K^-p at 3.9 and 4.6 GeV/c, 1.88 for K^-p at 10.1 GeV/c, and 0.63 for K^+n at 3 GeV/c. The plotted $d\sigma/dt$ in Fig. 9 have been multiplied by these numbers.

[24]We note that $\rho_{00}^{GJ}\, d\sigma/dt$ is significantly flatter than $\rho_{00}^{H}\, d\sigma/dt$ for $\bar{K}^{*0}$ production while the two have similar t dependence for the K^{*0} reaction. In the model this is associated with the relatively flat contribution of the π-ρ interference to $\rho_{00}^{GJ}\, d\sigma/dt$ which is constructive for $\bar{K}^{*0}$ and destructive for K^{*0}.

[25]The additional parameters inherent in such omissions may be used to improve the fit to the data at large t [cf. Fig. 1(b) especially]. However, this is not very meaningful until one has a better empirical understanding of the energy and momentum-transfer dependence of the data above $|t| = 0.5$ (GeV/c)^2; e.g., does $\rho_{00}^{H} d\sigma/dt$ have a dip or just a break at $|t| = 0.5$ (GeV/c)^2? Does it scale like $P_{\text{lab}}{}^{-3}$ there as in a simple Regge picture or like $P_{\text{lab}}{}^{-2}$ as for $d\sigma/dt$ at present energies? More generally, does $d\sigma/dt$ or $\rho\, d\sigma/dt$ exhibit shrinkage?

[26]M. Jacob and G. C. Wick, Ann. Phys. (N.Y.) 7, 404 (1959); G. C. Fox, dissertation, Cambridge, 1967 (unpublished).

[27]E. L. Berger and G. C. Fox, Nucl. Phys. B26, 1 (1971). See Eqs. (11)-(13) of this reference for a discussion of the absorption prescription (A1) and Eq. (14) for the signature factor (A9). The general definition of $h(s,b)$ in terms of $H^s(s,t)$ is given in Ref. 13.

[28]G. C. Fox and L. Sertorio, Phys. Rev. 176, 1739 (1968).

PHYSICAL REVIEW D VOLUME 4, NUMBER 9 1 NOVEMBER 1971

Proton-Antiproton Annihilation into $\pi^+\pi^-$ and K^+K^- from 700 to 1100 MeV/c*

M. A. Mandelkern, R. R. Burns, P. E. Condon, and J. Schultz
Department of Physics, University of California, Irvine, California 92664
(Received 26 July 1971)

Total and differential cross sections are presented for proton-antiproton annihilation into $\pi^+\pi^-$ and K^+K^- at six laboratory momenta between 686 and 1098 MeV/c. The two-pion final state displays moderate energy dependence in its differential cross section, but shows no evidence of any direct-channel resonances. In contrast, the two-kaon final state exhibits some behavior in the total and differential cross section suggestive of a possible direct-channel effect between 800 and 1000 MeV/c.

I. INTRODUCTION

It has been apparent for several years now that the meson spectrum above ~1 GeV/c^2 mass is extremely rich in states of assorted quantum numbers. This fact was established gradually during the past decade by a steady stream of discoveries, and demonstrated most dramatically, perhaps, by the results of the CERN Missing Mass Spectrometer experiments[1] which reported the R, S, T, U complexes of resonances with masses between 1690 and 2380 MeV/c^2. These reports have since been supplemented by many others. Aside from the apparent complexity of the spectrum, what is particularly interesting and even surprising is the extreme narrowness of the reported widths, with typical upper limits given at 30 MeV/c^2 or less. With such an abundance of very narrow massive bosons, it is tempting to speculate that perhaps some of the broader enhancements observed contain a complex fine structure as yet unresolved.

Resolving close, narrow resonances is a formidable task in bubble-chamber production experiments, where effective mass techniques are usually limited by resolutions of ~10 MeV/c^2 or more. However, in formation experiments, where the resonance appears as an s-channel enhancement, the obtainable resolution is considerably greater. In particular the proton-antiproton system potentially offers the possibility of observing nonstrange boson resonances with mass $\geq 2M_N$ with resolution of the order of a few MeV/c^2. To be specific, in the ex-